



Invited Article

Computational Fluid Dynamic Simulation of Single Bubble Growth under High-Pressure Pool Boiling Conditions

Janani Murallidharan ^a, Giovanni Giustini ^a, Yohei Sato ^{b,*}, Bojan Ničeno ^b, Vittorio Badalassi ^a, and Simon P. Walker ^a

^a Department of Mechanical Engineering, Imperial College London, London SW7 2AZ, UK

^b Nuclear Energy and Safety Research Department, Paul Scherrer Institute, Villigen PSI 5232, Switzerland

ARTICLE INFO

Article history:

Received 31 May 2016

Accepted 3 June 2016

Available online 22 June 2016

Keywords:

Bubble Growth Rate

Direct Numerical Simulation

High Pressure

Pool Boiling

ABSTRACT

Component-scale modeling of boiling is predominantly based on the Eulerian–Eulerian two-fluid approach. Within this framework, wall boiling is accounted for via the Rensselaer Polytechnic Institute (RPI) model and, within this model, the bubble is characterized using three main parameters: departure diameter (D), nucleation site density (N), and departure frequency (f). Typically, the magnitudes of these three parameters are obtained from empirical correlations. However, in recent years, efforts have been directed toward mechanistic modeling of the boiling process. Of the three parameters mentioned above, the departure diameter (D) is least affected by the intrinsic uncertainties of the nucleate boiling process. This feature, along with its prominence within the RPI boiling model, has made it the primary candidate for mechanistic modeling ventures. Mechanistic modeling of D is mostly carried out through solving of force balance equations on the bubble. Forces incorporated in these equations are formulated as functions of the radius of the bubble and have been developed for, and applied to, low-pressure conditions only. Conversely, for high-pressure conditions, no mechanistic information is available regarding the growth rates of bubbles and the forces acting on them. In this study, we use direct numerical simulation coupled with an interface tracking method to simulate bubble growth under high (up to 45 bar) pressure, to obtain the kind of mechanistic information required for an RPI-type approach. In this study, we compare the resulting bubble growth rate curves with predictions made with existing experimental data.

Copyright © 2016, Published by Elsevier Korea LLC on behalf of Korean Nuclear Society. This is an open access article under the CC BY-NC-ND license (<http://creativecommons.org/licenses/by-nc-nd/4.0/>).

* Corresponding author.

E-mail address: yohei.sato@psi.ch (Y. Sato).

<http://dx.doi.org/10.1016/j.net.2016.06.004>

1738-5733/Copyright © 2016, Published by Elsevier Korea LLC on behalf of Korean Nuclear Society. This is an open access article under the CC BY-NC-ND license (<http://creativecommons.org/licenses/by-nc-nd/4.0/>).

1. Introduction

Understanding, and having the ability to predict, the disposition and intensity of nucleate boiling are plainly of great importance in water-cooled nuclear reactor design and safety analysis. Void distribution influences “nuclear” matters such as neutron moderation, can affect chemistry and crud deposition, and has obvious heat transfer and surface temperature significance. The incorporation of a reasonable representation of nucleate boiling into general-purpose computational fluid dynamics (CFD) used for nuclear core modeling is a current major development area for authors of such codes.

Component-scale modeling of nucleate boiling is generally performed via a heat flux partitioning approach. The wall heat flux is represented by three components, namely, “normal” single-phase convection, evaporation, and “quenching”—the flow of relatively cool liquid toward the wall as it refills the volume previously occupied by a departing bubble. Semiempirical representations of these components rely primarily upon experimental observations to estimate the main parameters involved: the bubble departure frequency, bubble departure diameter, nucleation site density, and “normal” convective cooling of the surface between the bubbles. This approach was initially developed as a one-dimensional representation of wall boiling, and the formulation provides a relationship between the surface heat flux, wall temperature, and bulk fluid temperature (this framework is still being used extensively in system codes [1]). For the use of this model with present-day general-purpose CFD codes, this closure relation is modified to be a closure relation between the wall temperature and the near-wall fluid temperature. The thrust of current research in this framework is to incorporate better, more mechanistically accurate representations of the heat flux components and wall bubble characteristics (bubble size, departure frequency, etc.).

Increasingly sophisticated interface tracking CFD codes, incorporating interface mass transfer, are becoming able to generate quite high-fidelity predictions of such complex events. This makes the use of such codes a possible complement to reliance on experimental observation to obtain the empirical relations needed for component-scale modeling.

For obvious reasons, observations of boiling at high pressures tend to be much more limited than those at low pressures. Among other things, this requires much reliance in high-pressure component scale boiling modeling on extrapolations of data obtained at much lower pressures. Augmentation of pressure information, by the conduction of reliable high-pressure simulations, is thus a very desirable objective. As part of this, of course, it is important to be confident that the simulations themselves are indeed reliable.

We are fortunate that a set of high-pressure boiling measurements have recently been reported by Sakashita [2]. To our knowledge, there have not yet been any published attempts at simulating these. We attempt such a simulation in this study, which would also be the first publication of an attempt to simulate high-pressure boiling using the Parallel Simulator of BOILING phenomena (PSI-BOIL) code. Our particular focus will be on an attempt to predict correctly the

bubble growth rate, which is fundamental to most of the phenomena at issue.

In Section 2, we discuss the extant experimental evidence on bubble growth rates and earlier, largely analytical, attempts at predicting such growth. In Section 3, we provide a very brief summary of the modeling embodied within the PSI-BOIL code. The experiment of Sakashita [2] is outlined in Section 4, and the computed results are compared with it. Finally, conclusions are drawn in Section 5.

2. Bubble growth rate formulations

There have been a considerable number of experiments aimed at measuring bubble growth rates, both within the bulk of a superheated liquid and in a thin superheated layer adjacent to a surface.

Most were performed at constant wall heat flux conditions [3,4]. Lee et al [5] performed experiments with a constant wall temperature and studied pool boiling of R11 and R113 for saturated boiling conditions.

Semiempirical fitting of observed growth rates in these experiments generates a remarkably consistent form, along with quite uniform numerical scaling factors. The general form of the expression found is as follows:

$$R_p = AN_{ja}\sqrt{\alpha_l t} \quad (1)$$

Various publications proposed differing values for the constant A , such as $(12/\pi)^{0.5}$ [6], $\pi^{0.5}$ [7], and $2/(\pi)^{0.5}$ [4] ($N_{ja} < 100$; i.e., constant values of 1.95, 1.77, 1.13). These experiments were largely performed at atmospheric pressure.

At higher pressures, physical properties of water are quite different. Volume ratios for liquid and vapor can be two orders of magnitude lower, surface tension can be approximately an order of magnitude lower, and “contact” conditions between the heated surface and the liquid–vapor interface can be very different, as can be the heat transfer through the microlayer (if one exists at these conditions). The net result of all these is that the bubble growth rate is expected to be lower and the detachment radius much smaller.

Labuntsov et al [8] analyzed bubble growth rates for water at high pressures (up to 10 MPa) and reported a bubble growth rate given by the following correlation:

$$R_p = \sqrt{2\beta \cdot N_{ja} \cdot \alpha_l t} \quad (2)$$

where β is a numerical coefficient that includes the effect of the contact angle and the thickness of the conduction layer near the bubble base. Akiyama et al [9] carried out an experiment for water boiling on a horizontal 8-mm-diameter cylinder at pressures of 0.1–1.5 MPa. They reported that the bubble growth rate becomes lower with increasing pressure and that it could approximately be expressed by

$$R_p = fn(t^{0.2}) \quad (3)$$

at 1.5 MPa. This relation is quite different from Eqs. (1) and (2).

However, neither of these studies used high-resolution visualization techniques, and hence little quantification of the underlying phenomenon is provided.

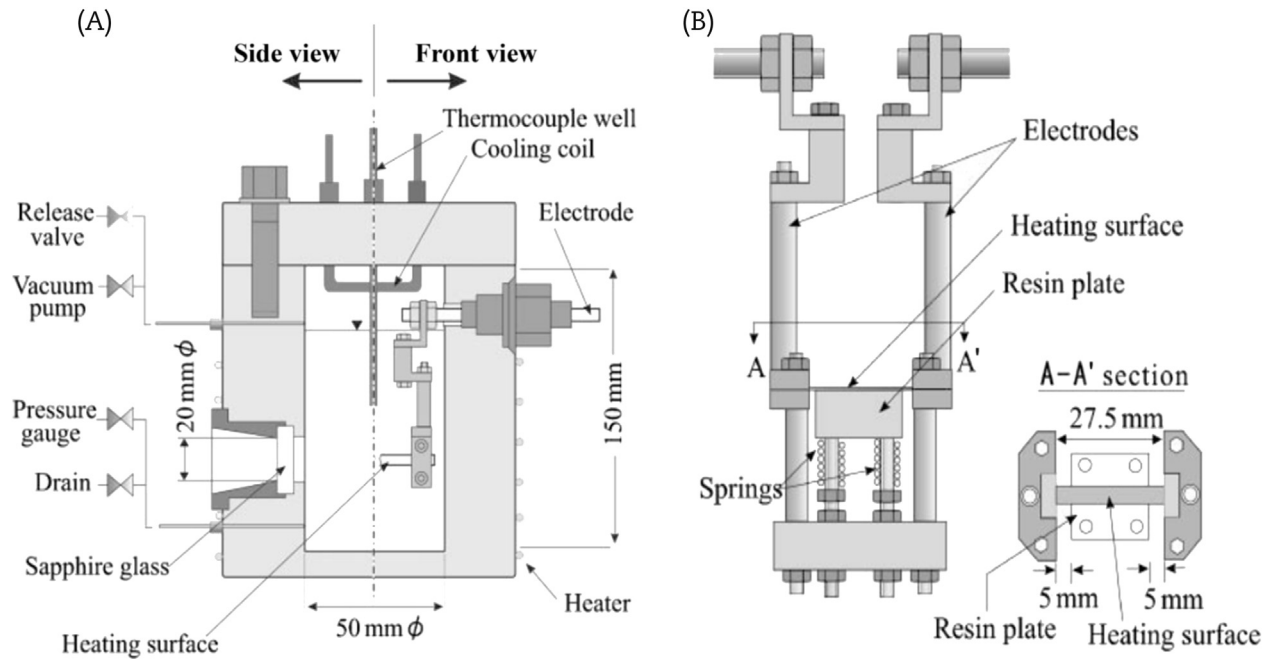


Fig. 1 – General view of Sakashita's experimental setup. (A) High-pressure cell. (B) Horizontal boiling test section [2].

3. Numerical method

3.1. General characteristics

PSI-BOIL is a direct numerical simulation code in which a single set of Navier–Stokes equations is solved under the assumption of an incompressible fluid based on a staggered finite-volume algorithm on Cartesian grids, using an interface tracking method together with a mass-conserving phase change model. It has been developed at PSI over several years and, as the name implies, focuses on the simulation of the boiling process. Further details of the code in general, and of the particular aspects outlined below that are of most relevance to the present study, are given in references [10,11].

3.2. Interface tracking

The color function is introduced as a volume fraction of liquid in a cell. The governing equation for the color function is the following:

$$\frac{\partial \phi}{\partial t} + \nabla \cdot (\phi \vec{u}) = -\dot{m} \frac{1}{\rho_l} \quad (4)$$

where \dot{m} is the mass transfer rate in $\text{kg/m}^3 \text{ s}$ computed in the phase change model. Here \dot{m} is positive for vaporization and negative for condensation. The derivation of Eq. (4) is given in Appendix A of reference [3]. The advection term is computed with the Constrained Interpolated Profile method: Conservative Semi-Lagrangian 2nd order scheme (CIP-CSL2) method, which features high accuracy in both mass conservation and

interface shape [12]. To avoid the smearing of the color function, a sharpening equation is employed:

$$\frac{\partial \phi}{\partial \tau} + \nabla \cdot (\phi(1-\phi)\vec{n}) = \nabla \cdot (\varepsilon \nabla \phi). \quad (5)$$

3.3. Surface tension model

In two-phase flows, modeling of the surface tension is an important factor. In PSI-BOIL, this is done using the “continuum surface force” (CSF) model developed by Brackbill et al [13] to represent the surface tension and wall adhesion forces. In this paper, this will be referred to as the “original” CSF model. There is a new, modified version of the CSF model that has been implemented based on the method proposed by Yokoi [14].

In the modified CSF model, curvature κ is firstly computed at the cell center:

$$\kappa = -(\nabla \cdot \vec{n}) \quad (6)$$

where \vec{n} is the unit normal vector to the liquid–vapor interface and defined at the cell center. Next, the curvature at the interface is computed using a linear interpolation. Then the curvature at the interface is extrapolated to cells around the interface, and the curvature used for the body force $\sigma \kappa \nabla \phi$ is based on the value at the interface.

The energy conservation equation can be written as follows:

$$C_p \left(\frac{\partial T}{\partial t} + \vec{u} \cdot \nabla T \right) = \nabla \cdot (\lambda \nabla T) + Q \quad (7)$$

The fundamental physical approximation/assumption made is that the liquid–vapor interface temperature is at the saturation temperature of the liquid. The normal

gradient of temperature of the liquid at the interface is computed to evaluate the heat flux, and from this the mass transfer. The conjugate heat transfer between the solid and fluid flow is taken into account using an immersed boundary method [15].

3.4. Microlayer model

A microlayer model is considered essential for CFD simulation of a bubble growing at the wall. This is required to model the thin liquid film that sometimes exists underneath growing bubbles. In the microlayer model [11] used in this study, the liquid microlayer thickness decreases and finally reaches a dry condition due to vaporization. Heat flux in the microlayer region is directly computed from the microlayer thickness, wall temperature, and the liquid–vapor interface temperature. The initial thickness of the microlayer, δ_0 , is given by the equation proposed by Utaka et al [16]:

$$\delta_0 = C_{slope} r_L \quad (8)$$

where r_L is the horizontal distance from a nucleation site to a certain point underneath a growing bubble and C_{slope} is a constant obtained from measurements. For instance, $C_{slope} = 4.46 \times 10^{-3}$ for water and $C_{slope} = 1.02 \times 10^{-2}$ for ethanol boiling from a heated quartz glass surface at atmospheric pressure. It should be emphasized that C_{slope} is the only empirical parameter for this model and is much more straightforward than other existing microregion models [17,18], in which several unknown parameters, such as the dispersion constant, adsorbed film thickness, gradient of the microlayer film thickness at the extremities of microregion, all need to be assigned appropriate values. Hereafter, we will use the value of C_{slope} measured for water by Utaka et al [16] and quoted above.

4. Results and discussion

4.1. Sakashita's high-pressure boiling experiment

The objective of Sakashita's [2] experiment was to make detailed observations of the boiling behavior on horizontal and vertical surfaces during saturated pool boiling of water at pressures from 0.35 MPa to 5 MPa. A general view of his setup can be seen in Fig. 1.

The high-pressure setup comprised a cylindrical cell with an inner diameter of 50 mm and a height of 150 mm. Sapphire windows were installed to enable the boiling phenomena to be observed, using a high-speed video camera and a microscope, with the video images analyzed manually. The measurements were predominantly of the nucleation site densities and the growth rates of the primary bubbles. For the current study, we will focus only on the horizontal surface experiments. The heating surface was a nickel foil, 8 μm thick, 3–4 mm wide, and 27.5 mm long. The heat-transfer surface was heated with a DC power supply, and the temperature of the heating surface was estimated from the change in the electric resistance of the nickel foil.

4.2. Conditions of simulation

The computational domain employed is a cuboid of dimension 0.150 mm \times 0.150 mm \times 0.158 mm, including an 8- μm -thick nickel heater at the bottom. All cases of the simulation were conducted for saturated pool boiling conditions. The fluid consists of water and steam at a system pressure of 44.7 bar. Material properties of the fluid and the condition of the heated wall are listed in Table 1. The simulation attempts to predict only the bubble growth from a seed on the wall and does not attempt to model the nucleation process itself. Consequently, the liquid near the wall is expected to be superheated at $t = 0$ seconds. Hence, an initial estimate of the thermal boundary layer thickness was made and applied. The simulations were carried out with the coarse grid of 262,144 cells (Table 2).

4.3. Parasitic currents

Fig. 2 is representative of the temperature contours obtained during the growth cycle of the bubble.

The interface temperature is assumed to be a constant, at the saturation temperature, in PSI-BOIL, and heat thus flows to this interface from the superheated bulk of the liquid. This heat flow is then associated with the generation of saturated vapor at the interface.

Velocity vectors at these locations indicate increased circulation and vortex-like structures. These are known as parasitic currents, by-products of the original CSF model used in these simulations, and are purely a numerical artifact. The parasitic currents are as a result of the large curvature (i.e., small bubble size, of the order of 10 μm), and they seem to cause increased heat transfer at the interface. In order to reduce the occurrence of these unphysical currents, the modified CSF model was implemented.

Fig. 3 shows the resulting temperature and velocity vectors, and it can be seen that the unphysical parasitic currents are significantly reduced. By comparing the temperature contours and velocity vectors of the original and modified CSF model simulations, some important effects of the presence of parasitic currents can be observed: (1) parasitic currents at the triple contact line cause a vapor plume to rise into a bubble, with the velocity vectors indicating that the speed of the vapor plume rising from the wall is high, and (b) the presence of parasitic currents results in cooler heater temperatures.

Table 1 – Fluid and solid material properties.

	Water	Steam
<i>Fluid properties at 44.7 bar</i>		
Dynamic viscosity (Pa sec)	1.03×10^{-4}	1.78×10^{-5}
Density (kg/m^3)	788.25	22.539
Specific heat ($\text{J}/\text{kg K}$)	4,949.3	4,214.5
Thermal conductivity ($\text{W}/\text{m K}$)	0.61293	0.053181
Surface tension coefficient (N/m)	0.024	
Expansion ratio ($\text{kg}/\text{m}^3 \text{ K}$)	–1.6	–0.101
<i>Solid properties: nickel</i>		
Density (kg/m^3)	8,908.0	
Specific heat ($\text{J}/\text{kg K}$)	444.0	
Thermal conductivity ($\text{W}/\text{m K}$)	90.9	

Table 2 – Computational grid.

Mesh	Grid A (coarse)	Grid B (medium)	Grid C (fine)
Minimum cell size (m)	2.00×10^{-6}	1.33×10^{-6}	1.00×10^{-6}
Number of cells	262,144	884,736	2,097,152
Computational domain (m ³): (1.58×10^{-4})	$(1.50 \times 10^{-4}) \times (1.50 \times 10^{-4}) \times (1.58 \times 10^{-4})$		

Further, in Fig. 4, measurement of the maximum lateral bubble radius in the 44.7 bar Sakashita test case is compared with the maximum lateral radius predicted by PSI-BOIL (maximum lateral radius indicates the maximum radius of the bubble in the direction parallel to the wall). It can be seen here that, although the presence of parasitic currents appears to modify the temperature and velocity contours, the bubble growth rates predicted by both the original CSF and the modified CSF model are similar to that observed in the experiment (Fig. 4B). For both cases, PSI-BOIL seems to achieve a very good prediction of the bubble growth rate at 44.7 bar.

4.4. Effect of microlayer

As mentioned earlier, PSI-BOIL was able to predict the growth rate of the bubble at a high pressure of 44.7 bar very well; however, it did not predict the time of detachment of the bubble accurately (Fig. 5). Detachment of the bubble from the wall is a very complex phenomenon. During detachment, the center of mass of the bubble begins to slowly move away from

the wall, while the base of the bubble still remains attached to it. This results in an elongation of the bubble in the wall-normal direction. The increase in bubble height in Fig. 5 is indicative of this phenomenon. When the bubble departs and the base of the bubble is no longer in contact with the wall, the bubble height parameter computed by PSI-BOIL will fall to zero or become equal to the height of the next seed bubble formed at the same cavity, as the case might be. Similarly, once the bubble departs completely from the wall, the maximum lateral radius becomes zero, and then, on nucleation of the next bubble in the same cavity, it becomes equal to the maximum lateral radius of the new seed bubble.

A likely cause for this lengthy predicted attachment of the bubble to the wall could be the microlayer model. The microlayer model implemented in PSI-BOIL, although a physically accurate model, contains an empirical multiplier C_{slope} (or) C_{utaka} , which is obtained from experiments conducted at atmospheric conditions. For high pressures, no microlayer experiments have been performed, and hence we do not know what this empirical value is at elevated pressures. Labuntsov et al [8] observed bubble behavior at a high pressure and theorized that bubble growth is primarily governed by the evaporation of liquid close to the bubble base. They postulated that as the excess enthalpy of the superheated bulk liquid surrounding the bubble is small at high pressures, the superheated layer would not contribute much to the evaporation. In this study, we investigate this issue using CFD simulations.

We also investigate whether the thickness of the microlayer is a likely cause for the delay in the bubble departure.

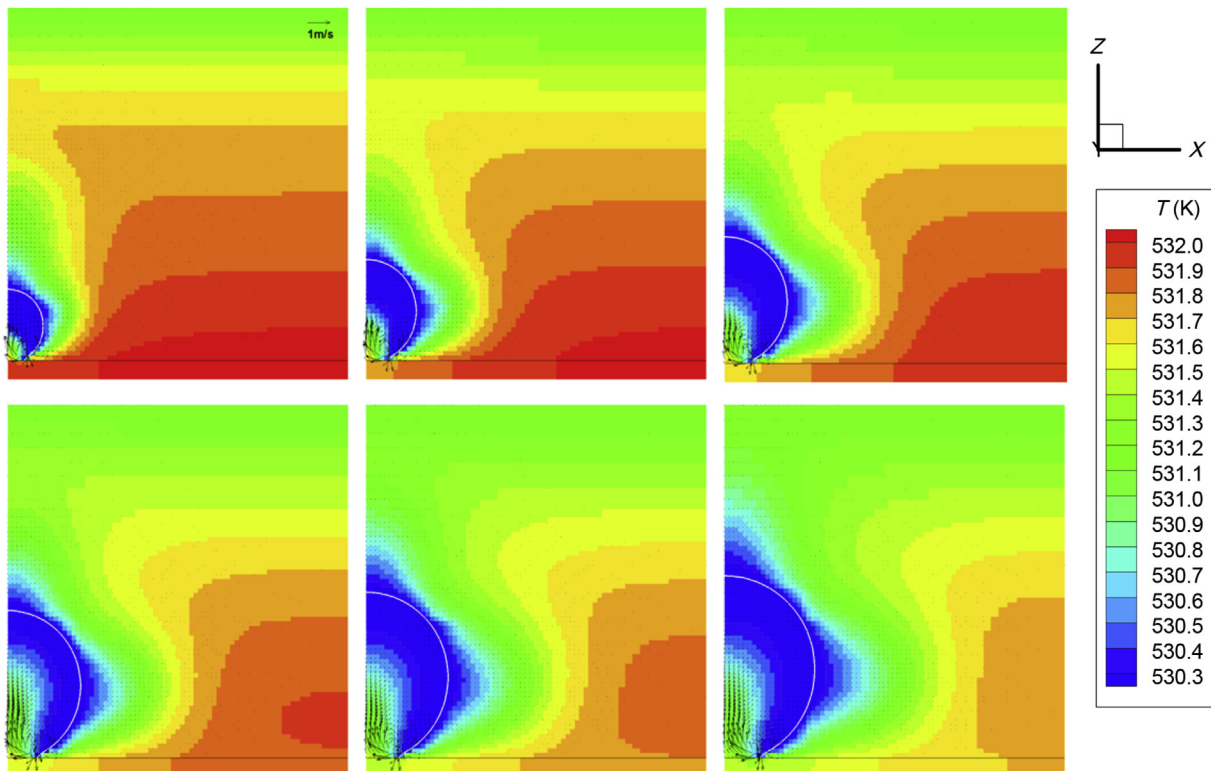


Fig. 2 – Parasitic currents: temperature contours and velocity vectors with original CSF model. Images are from $t = 0.002$ seconds to $t = 0.012$ seconds at every 0.002 seconds. CSF, continuum surface force.

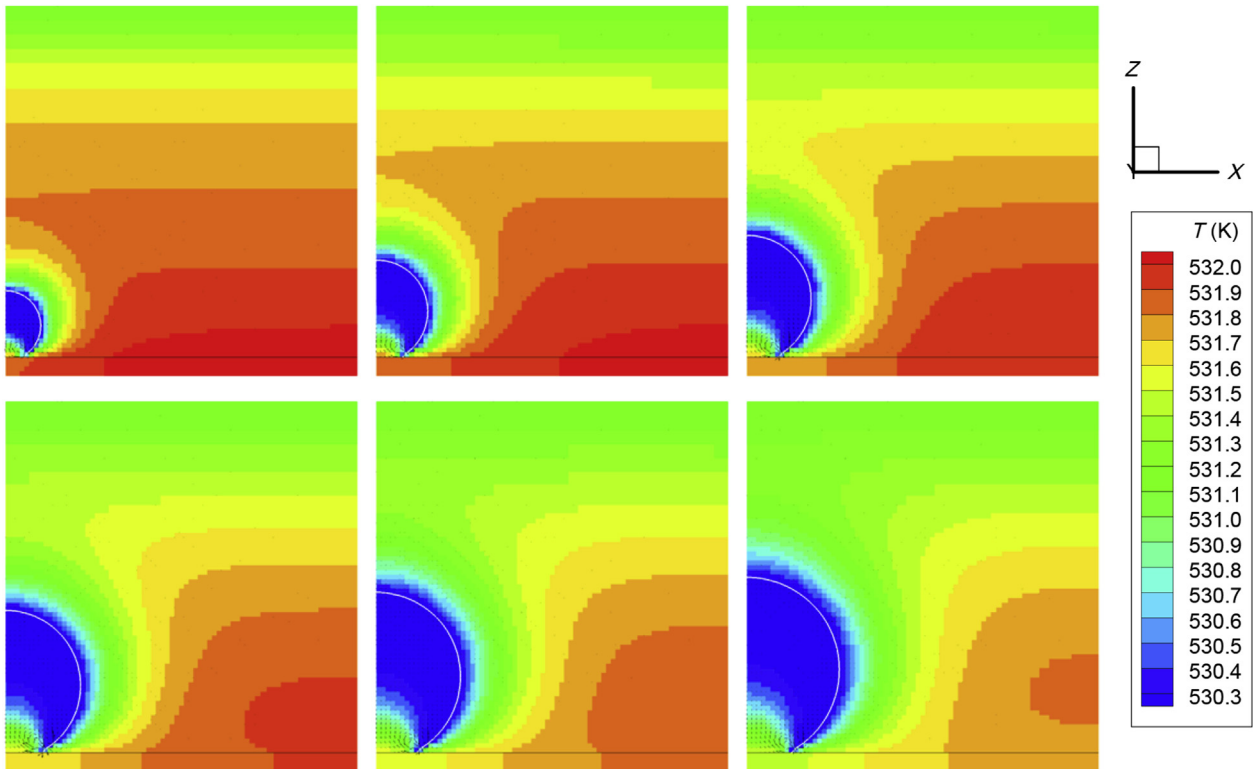


Fig. 3 – Reduced parasitic currents: temperature contours and velocity vectors with modified CSF model. Images are from $t = 0.002$ seconds to $t = 0.012$ seconds at every 0.002 seconds. CSF, continuum surface force.

Consequently, simulations are performed where (1) the size of the microlayer slope is reduced to 1/10 of its atmospheric value and (2) the microlayer model is completely removed.

The predicted bubble growth rate (Fig. 6), and the temperature and velocity plots do not vary much for the original

and reduced microlayer thickness. Time evolution of the temperature distribution with no microlayer (Fig. 7) is almost identical to the one with a microlayer (Fig. 3). This indicates that the presence of a microlayer model has little influence on bubble growth under these conditions (i.e., water at 45

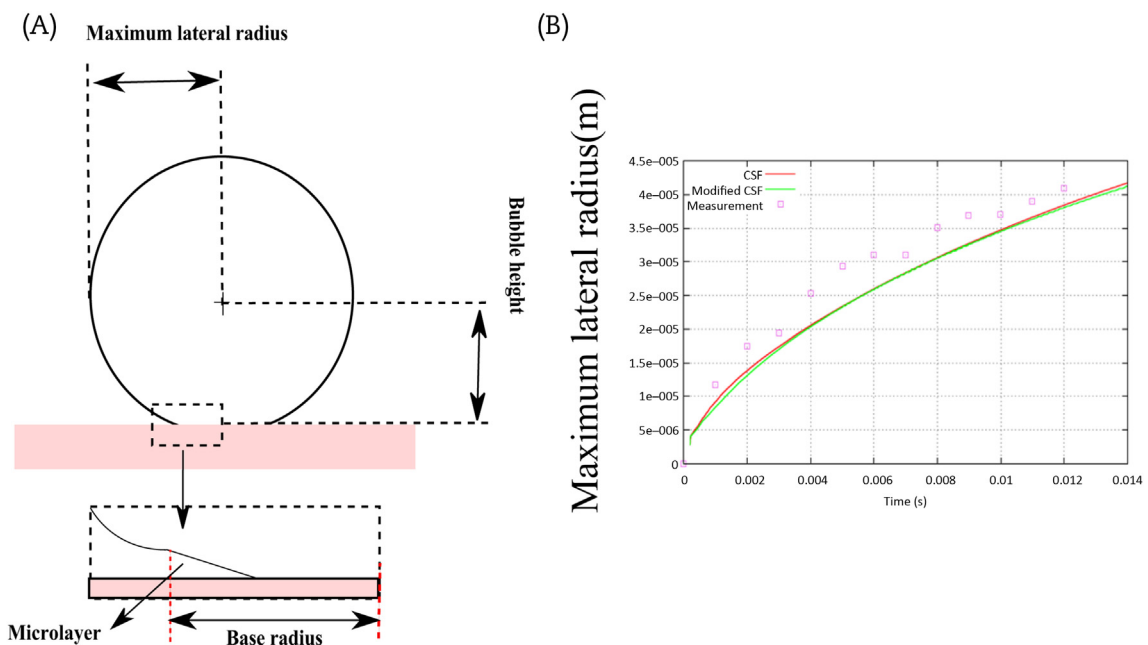


Fig. 4 – Bubble growth parameters. (A) Bubble dimensions. (B) Bubble growth rate predicted for 44.7 bar Sakashita test case. CSF, continuum surface force.

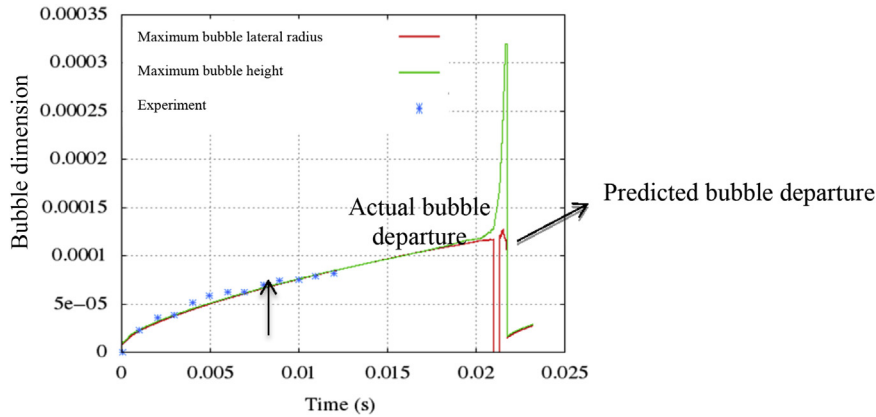


Fig. 5 – Bubble departure at 44.7 bar as predicted by PSI-BOIL.

bar). This is further supported by the fact that the rate of growth of the base radius of the bubble does not change with the presence of the microlayer (Fig. 6B). This could imply that the majority of the phase change occurs from the curved surface of the bubble, and only a negligible amount occurs from the microlayer region. Looking at the phase change rate for the no microlayer case (Fig. 8), it can clearly be seen that a large fraction of the phase change occurs near the triple contact line, but at the macrointerface level and not in the microlayer.

4.5. Comparison with Scriven bubble growth formulation

Bubbles at the wall grow in nonuniform temperature distributions. The temperature varies from the superheat temperature at the wall to the bulk liquid temperature at a certain (unknown) distance away from the wall, and this temperature variation is observed to affect the rate at which the bubble grows. In this section, the PSI-BOIL-predicted bubble growth rate is compared with that predicted by the Scriven's model for heat–diffusion controlled growth.

According to Scriven [19], the growth of the bubble radius in an infinite pool of liquid is proportional to the growth constant according to the following equation:

$$R(t) = 2\beta\sqrt{\alpha_1 t} \tag{9}$$

where α_1 is the thermal conductivity of the liquid, and the growth constant β is computed based on the temperature of the remote liquid and fluid properties.

For Sakashita's [2] high-pressure test case, no direct measurements of the temperature distribution near the heated wall are available. We have assumed that the bubbles grow in a superheated liquid layer in which the temperature decreases linearly with distance from the wall. The thickness of this superheated layer is assumed to be equivalent to the natural convection thermal boundary layer thickness and is determined using the following correlation:

$$\delta = 7.14 \left(\frac{\nu_1 \alpha_1}{g\beta\Delta T} \right)^{1/3} \tag{10}$$

Outside the layer, the liquid is assumed to be at the saturation temperature. As the bubble lift-off diameter is known from the experiment, it is possible to estimate the

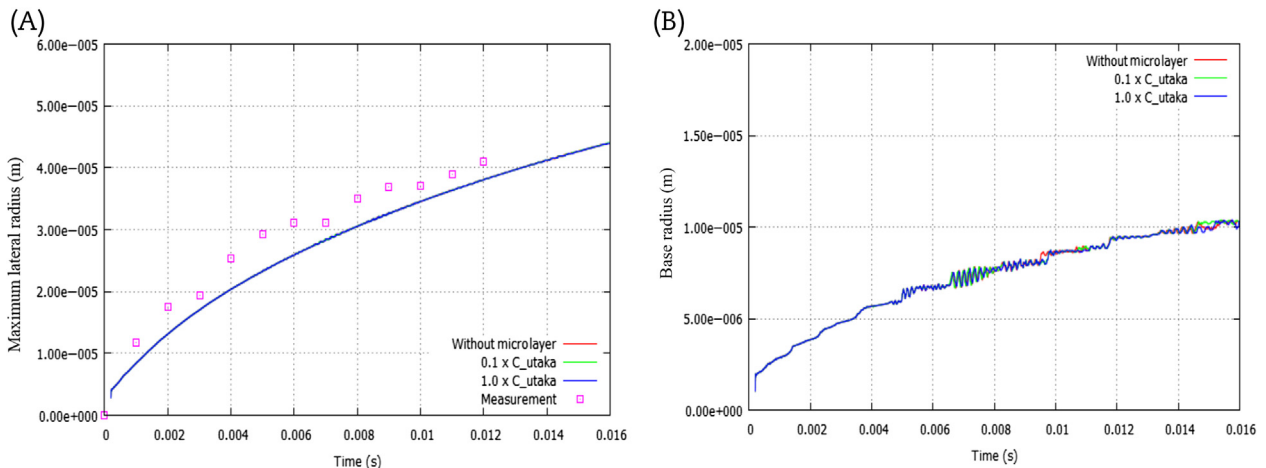


Fig. 6 – Effect of microlayer thickness. (A) Effect on maximum lateral radius. (b) Effect on base radius.

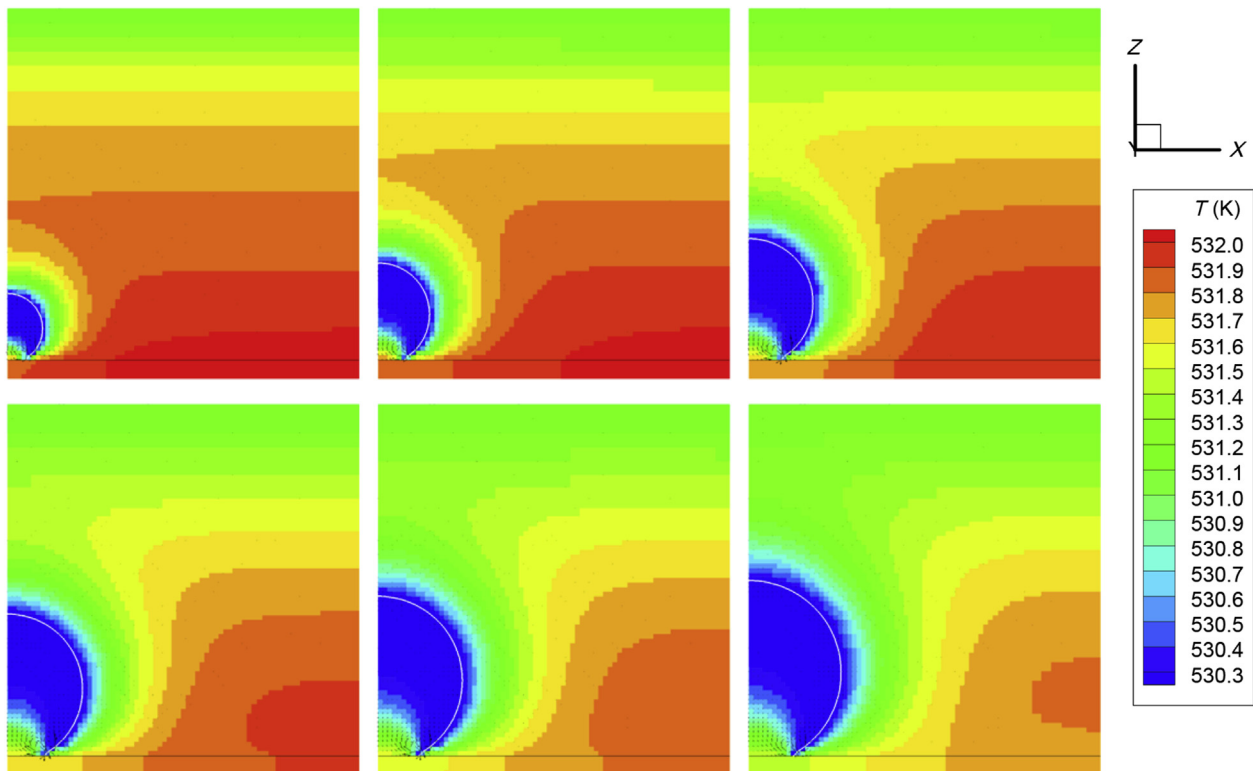


Fig. 7 – No microlayer: temperature contours and velocity vectors with modified CSF model. Images are from $t = 0.002$ seconds to $t = 0.010$ seconds at every 0.002 seconds. CSF, continuum surface force.

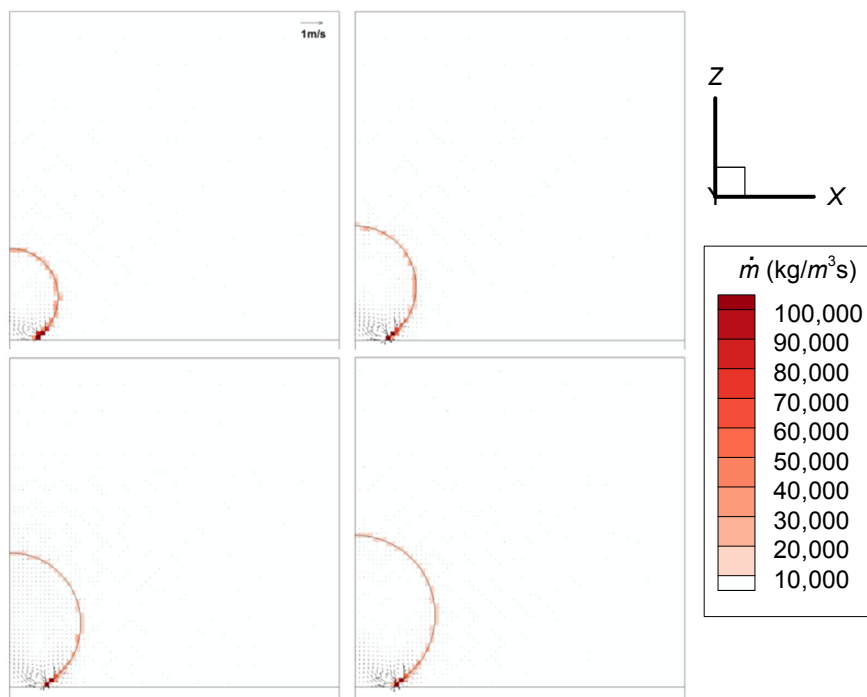


Fig. 8 – No microlayer: phase change rate distribution in kg/s m^3 from $t = 0.004$ seconds to 0.01 seconds at every 0.002 seconds.

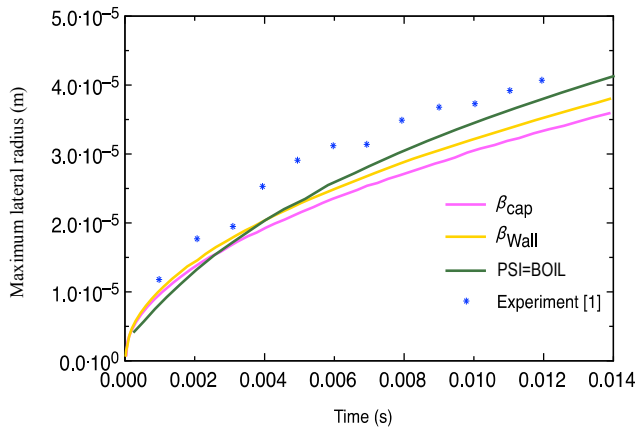


Fig. 9 – Comparison of 44.7 bar bubble growth prediction of PSI-BOIL (no microlayer) and Scriven's growth formulation [19].

temperature of the superheated liquid at a distance from the wall corresponding to the bubble cap elevation at the moment of detachment. The wall temperature and the temperature at the bubble cap elevation are the two limiting temperatures, which would influence the bubble growth rate, and Scriven's [19] treatment is applied to each of them. Growth constants are computed for superheats corresponding to the two limiting cases. In the first limiting case, the wall superheat at bubble inception is used to compute the growth constant β_w . In the second, the superheat at a distance from the wall equal to the lift-off diameter is used to compute the growth constant β_{cap} . A plot of the temporal variation of bubble radius for the two limiting cases is shown in Fig. 9. It can be seen that PSI-BOIL predicts the bubble growth rate at 44.7 bar better than the Scriven's [19] treatment for the two limiting cases.

4.6. Grid dependency test

In the PSI-BOIL code, the mass-transfer rate is directly computed from the heat flux coming to the liquid–vapor interface from the surrounding fluid or solid. The heat flux is

based on the temperature gradient, which is influenced by grid spacing, if a sufficiently small grid is not used. Thus, a grid dependency test is required. In addition, the seed bubble is initially hemispherical in shape, the radius being typically one cell width of the underlying grid. This means that the model is dependent on discretization (grid spacing), and a grid refinement study is then required; three grid levels are used to test it. The number of cells for each grid is listed in Table 2. As the bubble growth rate was found to be independent of the microlayer model, the grid dependency test was performed without the microlayer model. Fig. 10 shows the variation in the “maximum lateral radius” and the base radius of the growing bubble for each grid level. The growth rate of the maximum lateral radius increases with decreasing grid size. This tendency is considered reasonable because a smaller grid can evaluate the steep temperature gradient more accurately (i.e., the coarser grid underestimates the temperature gradient). Such a condition is observed around the liquid adjacent to the liquid–vapor interface. The base radius does not seem to vary greatly with grid size, indicating that the wall adhesion force implemented and defined in the CSF model is less dependent on grid spacing. Fig. 11 shows the difference in the temperature contours and velocity vectors for the different grid sizes.

5. Conclusions

- (1) The bubble growth rate predicted by PSI-BOIL agrees well with that of the 44.7-bar pool boiling experiment of Sakashita [2]. This indicates that PSI-BOIL can predict bubble growth rates at higher pressures and can be used to obtain the bubble growth rate expression for use in component scale boiling modeling. This is indeed the thrust of the work that is currently underway, wherein a growth rate equation applicable for different pressures is being developed.

For the current case, the bubble growth rate predicted by PSI-BOIL (and correlated by Sakashita [2]) is as follows:

$$R_p = C\sqrt{\alpha_l t} \quad (11)$$

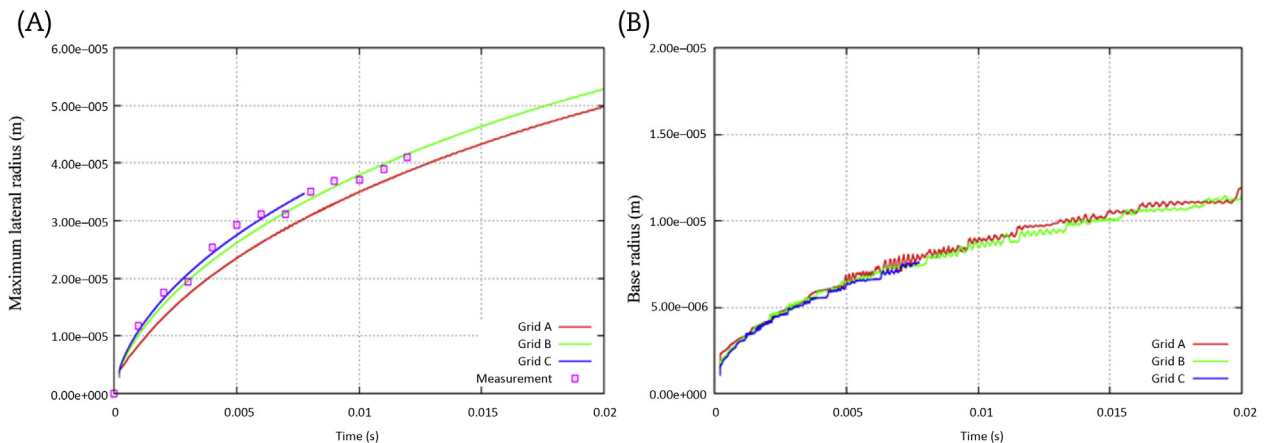


Fig. 10 – Grid dependency test. (A) Test for maximum lateral radius. (B) Test for base radius.

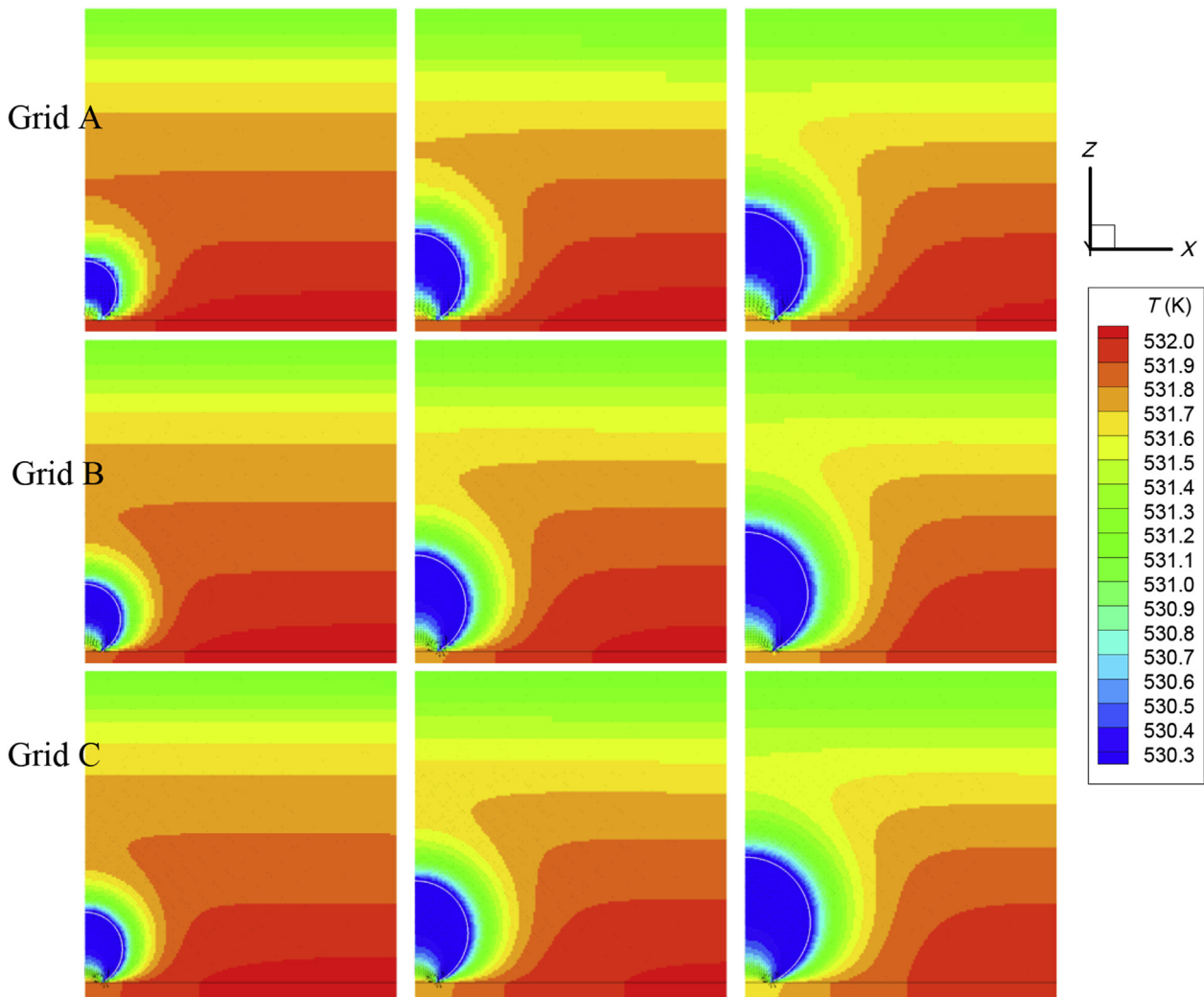


Fig. 11 – Grid dependency study: temperature contours and velocity vectors. Images are from $t = 0.002$ seconds to $t = 0.006$ seconds at every 0.002 seconds.

where $C = \sqrt{2\beta N_{ja}}$ and $\beta = 3$. This expression should perhaps be used for the component-scale bubble departure diameter modeling at 45 bar in place of the commonly used Plesset and Zwick [6] equation (which is applicable to atmospheric pressure). It is important to note that the growth rate at 45 bar varies as $\sqrt{N_{ja}}$ and not as N_{ja} (as it does at atmospheric pressure).

- (2) An unphysical temperature distribution is observed when the original CSF model is used due to strong parasitic currents. The parasitic currents result from the high curvature (i.e., small bubble size, of the order of $10 \mu\text{m}$). The unphysical temperature distribution is reduced considerably once the modified CSF model is used.
- (3) The presence of the microlayer model implemented in the PSI-BOIL code as well as its thickness has little influence on bubble growth for saturated pool boiling of water at 45 bar with respect to the maximum lateral radius of the bubble. It is observed from the simulations that the maximum phase change is observed near the triple contact line region, but at the macroscale level.

Consequently, from this study it is seen that the application of PSI-BOIL is not limited to augmentation of boiling models at the component scale level alone. It shows that the code can, in fact, provide a better understanding of the probable microscopic events that are responsible for the macro-scale phenomenon.

Conflicts of interest

All authors have no conflicts of interest to declare.

Acknowledgments

This work was supported through the EPSRC grant EP/I012427/1 as part of the Indo-UK collaboration and also partially supported by a grant from the Swiss National Supercomputing Centre (CSCS) under the project ID “psi”. Financial support to Giovanni Giustini from Rolls Royce is gratefully acknowledged.

Nomenclature

Variables	Meaning	Unit
A	Constant	–
C_p	Volumetric specific heat	$\text{J/m}^3\text{K}$
g	Gravitational acceleration	m/s^2
N_{Ja}	Jakob number	–
p	Pressure	N/m^2
Q	Heat source	W/m^3
R_p	Bubble radius	m
T	Temperature	K
t	Time	seconds
u	Velocity	m/s
Greek		
α	Thermal diffusivity	m^2/s
ε	Coefficient for interface thickness	m
ϕ	Color function	–
λ	Thermal conductivity	W/mK
ρ	Density	kg/m^3
τ	Pseudotime	–
B	Growth constant	–
N	Kinematic viscosity	m^2/s
Subscripts		
L	Liquid	

REFERENCES

- [1] Y. Lee, G. Park, TAPINS: a thermal–hydraulic system code for transient analysis of a fully-passive integral PWR, *Nucl. Eng. Technol* 45 (2013) 439–458.
- [2] H. Sakashita, Bubble growth rates and nucleation site densities in saturated pool boiling of water at high pressures, *J. Nucl. Sci. Technol* 48 (2011) 734–743.
- [3] C.H. Han, P. Griffith, The mechanism of heat transfer in nucleate pool boiling—Part I. Bubble initiation, growth and departure, *Int. J. Heat Mass Transf* 8 (1965) 887–904.
- [4] R. Cole, H.L. Shulman, Bubble growth rate at high Jakob numbers, *Int. J. Heat Mass Transf* 9 (1966) 1377–1390.
- [5] H.C. Lee, B.D. Oh, S.W. Bae, M.H. Kim, Single bubble growth in saturated pool boiling on a constant wall temperature surface, *Int. J. Multiphase Flow* 29 (2003) 1857–1874.
- [6] M.S. Plesset, S.A. Zwick, The growth of vapor bubbles in superheated fluids, *J. Appl. Phys* 25 (1954) 493–500.
- [7] H.K. Forster, N. Zuber, Growth of a vapor bubble in a superheated liquid, *J. Appl. Phys* 25 (1954) 474–478.
- [8] D.A. Labuntsov, B.A. Kol'chugin, V.S. Golovin, E.A. Zakharova, L.N. Vladimirova, Study of the growth of bubbles during boiling of saturated water within a wide range of pressures by means of high-speed moving pictures, *UCS 536.423 1* (1964) 404–409 [translated from *Teplofizika Vysokikh Temperatur* 2(1964) 446–453].
- [9] M. Akiyama, H. Tachibana, N. Ogawa, Effects of system pressure on bubble growth rate, *Trans, JSME* 35 (1969) 117–126 [In Japanese].
- [10] Y. Sato, B. Niceno, A sharp-interface phase change model for a mass-conservative interface tracking method, *J. Comput. Phys* 249 (2013) 127–161.
- [11] Y. Sato, B. Niceno, A depletable micro-layer for nucleate pool boiling, *J. Comput. Phys* 300 (2015) 20–52.
- [12] T. Nakamura, R. Tanaka, T. Yabe, K. Takizawa, Exactly conservative semi-Lagrangian scheme for multi-dimensional hyperbolic equations with directional splitting technique, *J. Comput. Phys* 174 (2001) 171–207.
- [13] J.U. Brackbill, D.B. Kothe, C. Zemach, A continuum method for modeling surface tension, *J. Comput. Phys* 100 (1992) 335–354.
- [14] K. Yokoi, A practical numerical framework for free surface flows based on CLSVOF method, multi-moment methods and density-scaled CSF model: numerical simulations of droplet splashing, *J. Comput. Phys* 232 (2013) 252–271.
- [15] B. Ničeno, F. Reiterer, A. Ylönen, H.M. Prasser, Simulation of single-phase mixing in fuel rod bundles, using an immersed boundary method, *Phys. Scr* 88 (2013) 1–13.
- [16] Y. Utaka, Y. Kashiwabara, M. Ozaki, Microlayer structure in nucleate boiling of water and ethanol at atmospheric pressure, *Int. J. Heat Mass Transf* 57 (2013) 222–230.
- [17] P.C. Stephan, C.A. Busse, Analysis of the heat transfer coefficient of grooved heat pipe evaporator walls, *Int. J. Heat Mass Transf* 35 (1992) 383–391.
- [18] J.H. Lay, V.K. Dhir, Shape of a vapor stem during nucleate boiling of saturated liquids, *J. Heat Transf* 117 (1995) 394–401.
- [19] L.E. Scriven, On the dynamics of phase growth, *Chem. Eng. Sci.* 10 (1959) 1–13.